

Constraining the mass of the graviton with the planetary ephemeris INPOP

L. Bernus¹, O. Minazzoli^{3,4}, A. Fienga^{2,1}, M. Gastineau¹, J. Laskar¹, P. Deram²

¹IMCCE, Observatoire de Paris, PSL University, CNRS, Sorbonne
Université, 77 avenue Denfert-Rochereau, 75014 Paris, France

²Géoazur, Observatoire de la Côte d’Azur, Université Côte
d’Azur, IRD, 250 Rue Albert Einstein, 06560 Valbonne, France

³Centre Scientifique de Monaco, 8 Quai Antoine 1er, Monaco

⁴Artemis, Université Côte d’Azur, CNRS, Observatoire de la Côte d’Azur, BP4229, 06304, Nice Cedex 4, France

We use the planetary ephemeris INPOP17b to constrain the mass of the graviton in the Newtonian limit. We also give an interpretation of this result for a specific case of fifth force framework. We find that the residuals for the Cassini spacecraft significantly (90% C.L.) degrade for Compton wavelengths of the graviton smaller than 1.83×10^{13} km, corresponding to a graviton mass bigger than $6.76 \times 10^{-23} \text{ eV}/c^2$. This limit is comparable in magnitude to the one obtained by the LIGO-Virgo collaboration in the radiative regime. We also use this specific example to illustrate why constraints on alternative theories of gravity obtained from postfit residuals are generically overestimated.

INTRODUCTION

From a particle physics point of view, general relativity can be thought as a theory of a massless spin-2 particle — hereafter named *graviton*. From this perspective, it is legitimate to investigate whether or not the graviton could actually possess a mass — even if minute. Such an eventuality has been scrutinized from a theoretical point of view since the late thirties, with the pioneer work of Fierz and Pauli [1]. There is a wide set of massive gravity theories, which lead to various phenomenologies [2]. One of the generic prediction from several models — although not all of them¹ — is that the usual $1/r$ falloff of the Newtonian potential acquires a Yukawa suppression [2]. In the present manuscript, we aim to test this particular phenomenology, regardless of the specificity of the theoretical model that produced it. For more information on the status of current theoretical models, we refer the reader to [2, 3]. As a consequence, we assume that the line element in a space-time curved by a spherical massive object at rest, at leading order in the Newtonian regime, reads

$$ds^2 = \left(-1 + \frac{2GM}{c^2 R} e^{-R/\lambda_g} \right) c^2 dT^2 + \left(1 + \frac{2GM}{c^2 R} e^{-R/\lambda_g} \right) dL^2, \quad (1)$$

with $dL^2 \equiv dX^2 + dY^2 + dZ^2$, $R \equiv \sqrt{X^2 + Y^2 + Z^2}$ and λ_g the Compton wavelength of the graviton — although we will see that our constraints can be applied on a wider range of massive and non-massive gravity metrics. Obviously, as long as λ_g is big enough, the gravitational

phenomenology in the Newtonian regime can reduce to the one of general relativity to any given level of accuracy.

Another generic feature of many massive gravity theories is that, if the graviton is massive, its dispersion relation may be modified according to $E^2 = p^2 c^2 + m_g^2 c^4$ [2], such that the speed of a gravitational waves depends on its energy (or frequency) $v_g^2/c^2 = c^2 p^2/E^2 \simeq 1 - h^2 c^2/(\lambda_g^2 E^2)$. Therefore, the waveform of gravitational waves would be modified during their propagation, while at the same time, sources of gravitational waves have been seen up to more than 1420 Mpc (at the 90% C.L.) [4]. As a consequence, waveform match filtering can be used to constrain the graviton mass from gravitational waves detections [5, 6].

Combining bounds from several events in the catalog GWTC-1 [4] leads to $\lambda_g \geq 2.6 \times 10^{13}$ km (resp. $m_g \leq 5.0 \times 10^{-23} \text{ eV}/c^2$ [4, 7]²) at the 90% C.L.³. It is important to keep in mind that this limit is obtained in the radiative regime, while we focus here on the Newtonian regime. Although, one could expect λ_g to have the same value in both regimes for most massive gravity theories, it may not be true for all massive gravity theories. Therefore, both constraints should be considered independently from an agnostic point of view. See, e.g., [2] for a review on the graviton mass constraints.

IMPORTANCE OF A GLOBAL FIT ANALYSIS

Twenty years ago [5] and more recently [8], Will argued that Solar System observations could be used to improve — or at least be comparable with — the constraints on λ_g obtained from the LIGO-Virgo Collabo-

¹ In particular, usually not for models prone to the Vainshtein mechanism [2].

² With the definition $m_g = h/(c\lambda_g)$.

³ Assuming that the graviton mass affects the propagation only, and not the binaries dynamics.

	λ_g	a Mercury	a Mars	a Saturn	a Venus	a EMB	GM_\odot
λ_g	1	0.50	0.49	0.04	0.39	0.05	0.66
a Mercure	...	1	0.21	0.001	0.97	0.82	0.96
a Mars	1	0.03	0.29	0.53	0.06
a Saturn	1	0.003	0.02	0.01
a Venus	1	0.86	0.94
a EMB	1	0.73
GM_\odot	1

TABLE I. Examples of correlations between various INPOP17b parameters and the Compton wavelength λ_g . a , EMB and M_\odot state for semi-major axes, the Earth-Moon barycenter and the mass of the Sun respectively.

ration — assuming that the parameters λ_g appearing in both the radiative and Newtonian limits are the same. A graviton mass would indeed lead to a modification of the perihelion advance of Solar System bodies. Hence, based on current constraints on the perihelion advance of Mars — or on the post-Newtonian parameters γ and β — derived from Mars Reconnaissance Orbiter (MRO) data, Will estimates that the graviton’s Compton wavelength should be bigger than $(1.2 - 2.2) \times 10^{14}$ km (resp. $m_g < (5.6 - 10) \times 10^{-24}$ eV/ c^2), depending on the specific analysis. However, as an input for his analysis, Will uses results based on the statistics of residuals of the Solar System ephemerides that are performed without including the effect of a massive graviton. But various parameters of the ephemeris (eg. masses, semi-major axes, Compton parameter, etc.) are all more or less correlated to λ_g (see Table I). Therefore, any signal introduced by $\lambda_g < +\infty$ — for instance, a modification of a perihelion advance — can in part be re-absorbed during the fit of other parameters that are correlated with the mass of the graviton. (See Supplemental Materials). This necessarily leads to a decrease of the constraining power of the ephemeris on the graviton mass with respect to postfit estimates. As a corollary, all analyses based solely on postfit residuals tend to overestimate the constraints on alternative theories of gravity due to the lack of information on the correlations between the various parameters. Eventually, one cannot produce conservative estimates of any parameter without going through the whole procedure of integrating the equations of motion and fitting the parameters with respect to actual observations — which is the very *raison d’être* of the ephemeris INPOP.

INPOP (Intégrateur Numérique Planétaire de l’Observatoire de Paris) [9] is a planetary ephemeris that is built by integrating numerically the equations of motion of the Solar System following the formulation of [10], and by adjusting to Solar System observations such as lunar laser ranging or space missions observations. In addition to adjusting the astronomical intrinsic parameters, it can be used to adjust parameters that encode deviations from general relativity [11–14], such as λ_g . The latest released version of INPOP, INPOP17a [15],

benefits of an improved modeling of the Earth-Moon system, as well as an update of the observational sample used for the fit [14] — especially including the latest Mars orbiter data. For this work we use an extension of INPOP17a, called INPOP17b, fitted over an extended sample of Messenger data up to the end of the mission, provided by [16].

In the present communication, our goal is to use the latest planetary ephemeris INPOP17b in order to constrain a hypothetical graviton mass directly at the level of the numerical integration of the equations of motion and the resulting adjusting procedure. By doing so, the various correlations between the parameters are intrinsically taken into account, such that we can deliver a conservative constraint on the graviton mass from Solar System observations — details about the global adjusting procedure are given in Supplemental Material.

MODELISATION FOR SOLAR SYSTEM PHENOMENOLOGY

Following Will [8], we develop perturbatively the potential in terms of r/λ_g , such that the line element (1) now reads

$$ds^2 = \left(-1 + \frac{2GM}{c^2 r} \left[1 + \frac{1}{2} \frac{r^2}{\lambda_g^2} \right] \right) c^2 dt^2 + \left(1 + \frac{2GM}{c^2 r} \left[1 + \frac{1}{2} \frac{r^2}{\lambda_g^2} \right] \right) dl^2 + \mathcal{O}(c^{-3} \lambda_g^{-2}), \quad (2)$$

albeit with a change of coordinate system ⁴

$$T = \frac{t}{\sqrt{1 + \frac{GM}{c^2 \lambda_g}}}, \quad X^i = \frac{x^i}{\sqrt{1 - \frac{GM}{c^2 \lambda_g}}} \quad (3)$$

The change of coordinate system is meant to get rid of the non-observable constant terms that appear in the line element Eq. (1) after expanding in terms of λ_g^{-1} . Considering a N-body system, the resulting additional acceleration to incorporate in INPOP’s code is

$$\delta a^i = \frac{1}{2} \sum_P \frac{GM_P}{\lambda_g^2} \frac{x^i - x_P^i}{r} + \mathcal{O}(\lambda_g^{-3}), \quad (4)$$

where M_P and x_P^i are respectively the mass and the position of the gravitational source P . In what follows, we make the standard assumption that the underlying theory is such that light propagates along null geodesics [3].

⁴ We assume that the underlying theory of gravity is covariant, such that this change of coordinates has no impact on the derivation of the actual *observables*.

From the null condition $ds^2 = 0$ and Eq. (2), the resulting additional Shapiro delay at the perturbative level reads

$$\delta T_{ER} = \frac{1}{2} \sum_P \frac{GM_P}{c^3 \lambda_g^2} \left[\vec{N}_{ER} \cdot \left(\vec{R}_{PR} R_{PR} - \vec{R}_{PE} R_{PE} \right) \right. \\ \left. + b_P^2 \ln \left(\frac{R_{PR} + \vec{R}_{PR} \cdot \vec{N}_{ER}}{R_{PE} + \vec{R}_{PE} \cdot \vec{N}_{ER}} \right) \right] + \mathcal{O}(c^{-3} \lambda_g^{-3}), \quad (5)$$

where $\vec{R}_{XY} = \vec{x}_Y - \vec{x}_X$, $R_{XY} = |\vec{R}_{XY}|$, $\vec{N}_{XY} = \vec{R}_{XY}/R_{XY}$ and $b_P = \sqrt{R_{PE}^2 - (\vec{R}_{PE} \cdot \vec{N}_{ER})^2}$. One can notice that the correction to the Shapiro delay scales as $(L_c/\lambda_g)^2$ with respect to the usual delay, where L_c is a characteristic distance of a given geometrical configuration. Given the old acknowledged constraint from Solar System observations on the graviton mass ($\lambda_g > 2.8 \times 10^{12}$ km [5, 8, 17]), one deduces that the correction from the Yukawa potential on the Shapiro delay is negligible for past, current and forthcoming radio-science observations in the Solar System⁵.

On the other hand, the fifth force formalism predicts an additional Yukawa term to the Newtonian potential [18]

$$V = \frac{Gm}{r} (1 + \alpha e^{-r/\lambda}) \quad (6)$$

If we assume that $\lambda \gg r$ and $\alpha > 0$, we can also expand the Yukawa term, such that our result on λ_g can be transposed to $\lambda/\sqrt{\alpha}$ — although, one first has to rescale the gravitational constant to $\bar{G} = G(1+\alpha)$, and then to make the same coordinates change as in Eq. (3), but substituting λ_g by λ/α . Note that a fifth force is also one of the generic features of several massive gravity theories [2].

EVALUATION OF THE SIGNIFICANCE OF THE RESIDUALS DETERIORATION

To give a confidence interval for λ_g , we proceed as follows. For each value of λ_g , we perform a global fit of all other parameters to observations using the same data that for the reference solution INPOP17b — therefore, for the same number of observations. After the global fit procedure, we compute the residuals at the same dates that for the reference solutions and look how they are degraded or improved with respect to λ_g . The result is that Cassini residuals are the first to degrade significantly while λ_g decreases (see Supplemental Material for details).

⁵ However, note that the scaling of the correction to the Shapiro delay illustrates the breakdown of the λ_g^{-1} development in cases where the characteristic distances involved are large with respect to the Compton wavelength — as it should be expected.

To quantify the statistical meaning of this degradation, we perform a Pearson [19] χ^2 test between both residuals in order to look at the probability that they were both built from the same distribution. To compute the χ^2 , we build an optimal histogram with the Cassini residuals of INPOP17b using the method described in [20], assuming the gaussianity of the distribution of the residuals. We determine the optimal bins in which are counted the residuals to build the histogram. Then, using the same bins, we build an histogram for the Cassini residuals obtained by the solution to be tested with a given value of λ_g . Note that the first bin left-borned is $-\infty$ and the last bin right-borned is $+\infty$. Let $(C_i)_i$ be the bins in which are counted the values of the residuals and N_i^I , N_i^G be the number of residuals of INPOP17b and the solution to be tested, respectively, counted in bin number i . One can then compute

$$\chi^2(\lambda_g) = \sum_{i=1}^n \frac{(N_i^G - N_i^I)^2}{N_i^I} \quad (7)$$

For Cassini data, it occurs that the optimal binning gives 10 bins. As a result, this χ^2 follows a χ^2 law with 10 degrees of freedom. If the computed χ^2 is then greater than its quantile for a given confidence probability p , we can say that the distribution of the residuals obtained for λ_g is different from the residuals obtained by the reference solution with a probability p . This test can be done for both a positive detection of a physical effect and a rejection of the existence of a physical effect. If the computed $\chi^2(\lambda_g)$ becomes then greater than its critical value for a probability p , one has to check if residuals are smaller or bigger than those obtained by the reference solution. In the first case (smaller – or better – residuals), it means that the added effect increases significantly the quality of the residuals and is probably (with a probability p) a true physical effect. On the contrary, in the second case (bigger – or degraded – residuals), it means that the added effect is probably physically false. In our work, the critical increasing of $\chi^2(\lambda_g)$ corresponds to a degradation of the residuals (see Supplemental Material for a detailed analysis). The massive graviton can then be rejected for high enough values of the mass (or low enough values of λ_g).

RESULTS

In Fig. 1 we plot the χ^2 as a function of λ_g . In this plot, we give two values of quantiles associated to two probabilities of significance, $p = 90\%$ and $p = 99,9999999\%$, which correspond to critical values of χ^2 equal to 15.99 and 62.94 respectively for a 10 degrees of freedom χ^2 distribution. We obtain respectively $\lambda_g > 1.83 \times 10^{13}$ km (resp. $m_g < 6.76 \times 10^{-23}$ eV/ c^2) and $\lambda_g > 1.66 \times 10^{13}$ km (resp. $m_g < 7.45 \times 10^{-23}$ eV/ c^2). These results are shown

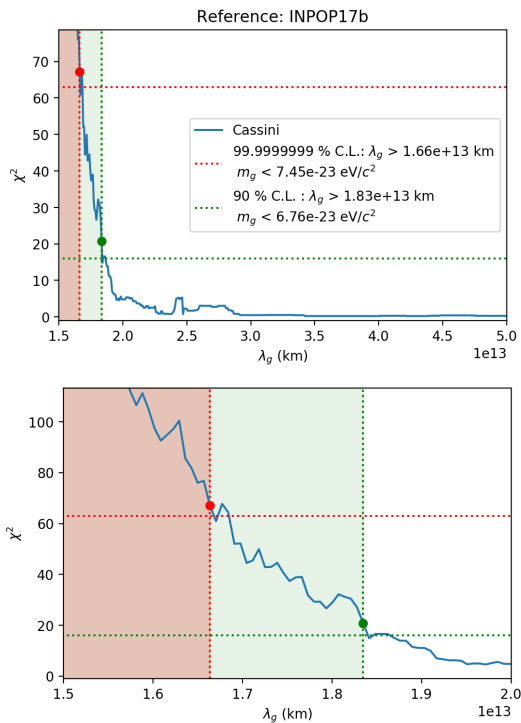


FIG. 1. Plot of $\chi^2(\lambda_g)$ and the constraints deduced for λ_g . The probabilities $p = 90\%$ and $p = 99,9999999\%$ correspond to critical values of χ^2 equal to respectively 15.99 and 62.94.

in Fig. 1. We also provide a zoom of the main figure in order to show that the χ^2 is not monotonic for small differences of λ_g . However, if a given limit is crossed several times, our algorithm automatically takes the most conservative value in the discrete set of λ_g , as can be seen in Fig. 1.

CONCLUSION

In the present manuscript, we deliver the first conservative estimate of the graviton mass from an actual fit of a combination of Solar System data, using a criterion based on a state of the art Solar System ephemerides: INPOP17b. The bound reads $\lambda_g > 1.83 \times 10^{13}$ km (resp. $m_g < 6.76 \times 10^{-23}$ eV/ c^2) with a confidence of 90% and $\lambda_g > 1.66 \times 10^{13}$ km (resp. $m_g < 7.45 \times 10^{-23}$ eV/ c^2) with a confidence of 99.9999999%. As previously explained, in terms of a fifth force, the constraint on λ_g can be translated into a constraint on $\lambda/\sqrt{\alpha}$, simply by substituting λ_g by $\lambda/\sqrt{\alpha}$, if $\alpha > 0$.

The fact that our 90% C.L. bound is comparable in magnitude to the one obtained by the LIGO-Virgo collaboration in the radiative regime [7, 21] is a pure coincidence: the two bounds rely on totally different types of observation — gravitational waves versus radioscience

in the Solar System — and probe different aspects of the massive graviton phenomenology — radiative versus Keplerian.

-
- [1] M. Fierz and W. Pauli, “On Relativistic Wave Equations for Particles of Arbitrary Spin in an Electromagnetic Field,” *Proceedings of the Royal Society of London Series A* **173**, 211–232 (1939).
 - [2] C. de Rham, J. T. Deskins, A. J. Tolley, and S.-Y. Zhou, “Graviton mass bounds,” *Reviews of Modern Physics* **89**, 025004 (2017), arXiv:1606.08462.
 - [3] C. de Rham, “Massive Gravity,” *Living Reviews in Relativity* **17**, 7 (2014), arXiv:1401.4173 [hep-th].
 - [4] The LIGO Scientific Collaboration, the Virgo Collaboration, B. P. Abbott, R. Abbott, T. D. Abbott, S. Abraham, F. Acernese, K. Ackley, C. Adams, R. X. Adhikari, and et al., “GWTC-1: A Gravitational-Wave Transient Catalog of Compact Binary Mergers Observed by LIGO and Virgo during the First and Second Observing Runs,” arXiv e-prints (2018), arXiv:1811.12907 [astro-ph.HE].
 - [5] C. M. Will, “Bounding the mass of the graviton using gravitational-wave observations of inspiralling compact binaries,” *Phys. Rev. D* **57**, 2061–2068 (1998), gr-qc/9709011.
 - [6] W. Del Pozzo, J. Veitch, and A. Vecchio, “Testing general relativity using Bayesian model selection: Applications to observations of gravitational waves from compact binary systems,” *Phys. Rev. D* **83**, 082002 (2011), arXiv:1101.1391 [gr-qc].
 - [7] The LIGO Scientific Collaboration and the Virgo Collaboration, “Tests of General Relativity with the Binary Black Hole Signals from the LIGO-Virgo Catalog GWTC-1,” arXiv e-prints, arXiv:1903.04467 (2019), arXiv:1903.04467 [gr-qc].
 - [8] Clifford M Will, “Solar system versus gravitational-wave bounds on the graviton mass,” *Classical and Quantum Gravity* **35**, 17LT01 (2018).
 - [9] A. Fienga, H. Manche, J. Laskar, and M. Gastineau, “INPOP06: a new numerical planetary ephemeris,” *Astronomy and Astrophysics* **477**, 315–327 (2008).
 - [10] T. D. Moyer, *Deep Space Communications and Navigation Series*, Vol. 2 (John Wiley & Sons, Inc., Hoboken, NJ, USA, 2003).
 - [11] A. Fienga, J. Laskar, P. Kuchynka, H. Manche, G. Desvignes, M. Gastineau, I. Cognard, and G. Theureau, “The INPOP10a planetary ephemeris and its applications in fundamental physics,” *Celestial Mechanics and Dynamical Astronomy* **111**, 363–385 (2011), arXiv:1108.5546 [astro-ph.EP].
 - [12] A. K. Verma, A. Fienga, J. Laskar, H. Manche, and M. Gastineau, “Use of MESSENGER radioscience data to improve planetary ephemeris and to test general relativity,” *Astronomy and Astrophysics* **561**, A115 (2014), arXiv:1306.5569 [astro-ph.EP].
 - [13] A. Fienga, J. Laskar, P. Exertier, H. Manche, and M. Gastineau, “Numerical estimation of the sensitivity of INPOP planetary ephemerides to general relativity parameters,” *Celestial Mechanics and Dynamical Astronomy* **123**, 325–349 (2015).
 - [14] V. Viswanathan, A. Fienga, O. Minazzoli, L. Bernus,

- J. Laskar, and M. Gastineau, “The new lunar ephemeris INPOP17a and its application to fundamental physics,” *MNRAS* **476**, 1877–1888 (2018), [arXiv:1710.09167 \[gr-qc\]](#).
- [15] V. Viswanathan, A. Fienga, M. Gastineau, and J. Laskar, “INPOP17a planetary ephemerides,” *Notes Scientifiques et Techniques de l’Institut de Mecanique Celeste* **108** (2017), last Accessed: 2018-11-13.
- [16] A. K. Verma and J.-L. Margot, “Mercury’s gravity, tides, and spin from MESSENGER radio science data,” *Journal of Geophysical Research (Planets)* **121**, 1627–1640 (2016), [arXiv:1608.01360 \[astro-ph.EP\]](#).
- [17] C. Talmadge, J.-P. Berthias, R. W. Hellings, and E. M. Standish, “Model-independent constraints on possible modifications of Newtonian gravity,” *Physical Review Letters* **61**, 1159–1162 (1988).
- [18] A. Hees, T. Do, A. M. Ghez, G. D. Martinez, S. Naoz, E. E. Becklin, A. Boehle, S. Chappell, D. Chu, A. Dehghanfar, K. Kosmo, J. R. Lu, K. Matthews, M. R. Morris, S. Sakai, R. Schödel, and G. Witzel, “Testing General Relativity with Stellar Orbits around the Supermassive Black Hole in Our Galactic Center,” *Physical Review Letters* **118**, 211101 (2017), [arXiv:1705.07902](#).
- [19] Karl Pearson, “On the criterion that a given system of deviations from the probable in the case of a correlated system of variables is such that it can be reasonably supposed to have arisen from random sampling,” in *Breakthroughs in Statistics: Methodology and Distribution*, edited by Samuel Kotz and Norman L. Johnson (Springer New York, New York, NY, 1992) pp. 11–28.
- [20] DAVID W. SCOTT, “On optimal and data-based histograms,” *Biometrika* **66**, 605–610 (1979).
- [21] B. P. Abbott, R. Abbott, T. D. Abbott, F. Acernese, K. Ackley, C. Adams, T. Adams, P. Addesso, R. X. Adhikari, V. B. Adya, and et al., “GW170104: Observation of a 50-Solar-Mass Binary Black Hole Coalescence at Redshift 0.2,” *Physical Review Letters* **118**, 221101 (2017), [arXiv:1706.01812 \[gr-qc\]](#).

Supplemental materials: Constraining the mass of the graviton with the planetary ephemeris INPOP

L. Bernus ¹, O. Minazzoli ^{3,4}, A. Fienga ^{2,1}, M. Gastineau ¹, J. Laskar ¹, P. Deram ²

¹IMCCE, Observatoire de Paris, PSL University, CNRS, Sorbonne Université, 77 avenue Denfert-Rochereau, 75014 Paris, France

²Géoazur, Observatoire de la Côte d’Azur, Université Côte d’Azur, IRD, 250 Rue Albert Einstein, 06560 Valbonne, France

³Centre Scientifique de Monaco, 8 Quai Antoine 1er, Monaco

⁴Artemis, Université Côte d’Azur, CNRS, Observatoire de la Côte d’Azur, BP4229, 06304, Nice Cedex 4, France

NUMERICAL ANALYSIS

To model and confront the massive graviton to Solar System observations, we add its contribution to the INPOP17b Solar System model (including asteroid masses), and then fit the newly obtained ephemeris according to the procedure described in [1]. For a fixed value of λ_g , we fit the parameters of the whole model to the data.

We have performed an iterative fit of the INPOP17b parameters of the ephemeris for each given values of λ_g . In order to compare the tested and the reference solutions, one needs to apply exactly the same procedure in each case. Accordingly, the same data and weights are used. As usual, weights are representative of data uncertainty and distribution. The comparison between the residuals of a solution with a massive graviton to the residuals of the reference solution gives a measurement of the sensibility of the ephemeris to the effects of a massive graviton. For each value of λ_g we compute the standard deviation of the residuals of range observations. More specifically, we exhibit residuals obtained with observations for Cassini mission, Messenger mission, and Mars Odyssey and Mex mission. Other observations are less relevant due to less accurate data and/or high correlation with λ_g . This algorithm processes for 1024 different fixed values of λ_g between 1×10^{13} and 8×10^{13} km. We plot the different standard deviations with respect to λ_g for each iteration. We remove the values of the reference solution standard deviations ¹ listed in Table I. In Table I, we indeed give the 1σ standard deviations of INPOP17b residuals together with the 1σ differences obtained between INPOP17b and the Jet Propulsion Laboratory ephemeris DE436 ² geocentric distances on the time interval of the data sample. The latter gives an idea of the internal accuracy of the reference ephemeris itself. At about the 10th iteration, the standard deviations for the three sets of residuals stop evolving — meaning that the adjustment has converged. We report the plot of the

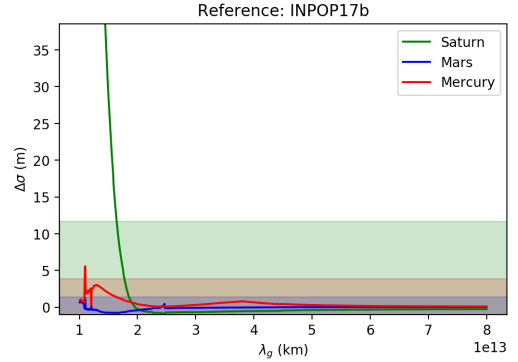


FIG. 1. Plot of the standard deviations with respect to λ_g after 12 iterations of the data fit. The values of the reference solution INPOP17b standard deviations (given in Table I) have been removed. The colored areas correspond to zones where the standard deviations of each observable are considered a priori as being marginally to not significant. The limits come from the estimation of the internal accuracy of the ephemeris obtained through the comparison with DE436, see Table I as well as text below. [A rigorous evaluation of the significance of the deterioration is made in the main part of the manuscript.]

standard deviations of the last iteration (the 13th) in Fig. 1.

An important point to have in mind is that Mars data constrain the global fit of parameters to observations — thanks to the important weight in the fit given to the Mars Odyssey and MEX missions accurate data in the reference solution ³. So, while in Will’s analysis [3], the high quality of Martian data is expected to allow the best constraints on λ_g , this high quality actually helps to better adjust the whole set of parameters — but they do not significantly constrain λ_g . Alternatively, given the fact that Saturn’s semi-major axis is less correlated to λ_g (see Table I in the main part of the manuscript), it is not surprising to see in Fig. 1 that Saturn positions

¹ i.e. for $\lambda_g = +\infty$

² Which is based on DE430 ([2]).

³ As mentioned above, weights are representative of data uncertainty and distribution.

Observations	Time Intervals	#	(O-C) INPOP17b	INPOP17b-DE436
			1σ [m]	1σ [m]
Mercury (Messenger)	2011 : 2013.2	950	7.2	3.9
Mars (Ody, MEX)	2002 : 2016.4	52946	5.0	1.4
Saturn (Cassini)	2004 : 2014	175	32.1	11.7

TABLE I. Summary of data selected for monitoring INPOP sensitivity to λ_g . Columns 2 and 3 provide the time coverage of the sample and the number of observations per sample respectively. Column 4 gives the 1σ standard deviation of residuals obtained with INPOP17b. These standard deviations are taken as reference values in the text. The last column indicates the 1σ differences between INPOP17b and DE436 for geocentric distances and for interval of time covered by the two ephemeris adjustments.

deduced from the Cassini observations are actually the most constraining on λ_g .

It is found that the variation of the standard deviations of the selected residuals dominates compared to the variations of the mean values of the residuals, for all values of λ_g . Therefore, in the following, we focus on standard deviations of data.

As one can see in Fig. 1, after 12 iterations, only residuals deduced from Saturn positions obtained with Cassini show important deviations at a high value of λ_g . On the other hand, all the values of standard deviation of Mars data are below 1.5 m higher than the reference value. Around $\lambda_g = 1.5 \times 10^{13}$ km, Messenger data go a little above 3 m higher than the reference value, but decrease then as λ_g decreases, while Mars standard deviation does exactly the opposite — indicating a compensating mechanism between the two sets of standard deviations, whose controlling parameters are indeed highly correlated. Of course, the compensating mechanism is actually across the whole set of residuals and depends on both the weights attributed to the different data and to the correlations between various parameters. In the end, only residuals deduced from Cassini show a significant (and monotonic) increase as λ_g decreases, as one can see in Fig. 1.

DISCUSSION

The significant level of correlation between λ_g and the Solar System parameters indicates that any signal introduced by $\lambda_g < +\infty$ can in part be re-absorbed during the fit of all the parameters. As a consequence, as explained previously, analyses based on postfit residuals tend to overestimate the constraint on λ_g . We can illustrate this further with the following example.

We look at the standard deviations of residuals with respect to λ_g without re-adjusting all the Solar System parameters — which effectively corresponds to do a sort of postfit analysis, in the sense that one considers Solar System parameters to be given beforehand by previous analyses. This gives an indication of the amplitude of

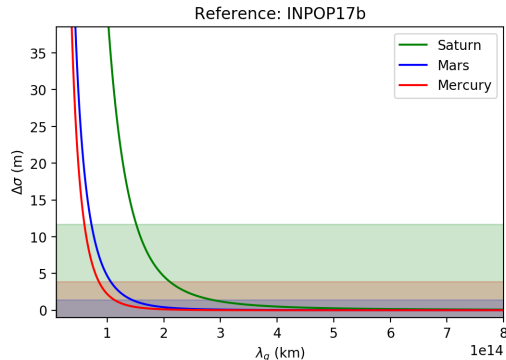


FIG. 2. Plot of the standard deviations variations with respect to λ_g without adjusting the Solar System parameters. As expected, λ_g seems to have a much more important impact compared to the case in Fig. 1, where one has adjusted the Solar System parameters after adding the λ_g parameter. [Note that the scale of the x-axis here is different with respect to Fig. 1].

the effect of $\lambda_g < +\infty$ on the ephemeris, when the Solar System parameters are (wrongly) considered to be known beforehand. The standard deviations for Saturn Cassini residuals are shown in Fig. 2. If one applies the same statistical analysis on those residuals — instead of on the residuals obtained after adjusting the Solar System parameters as in Fig. 1 of the main part of the manuscript — one would mistakenly get at an improvement of more than a factor 20 on the constraint of λ_g , as it can be seen in Fig. 3 (the postfit analysis gives $\lambda_g \leq 4.98 \times 10^{14}$ km instead of 1.83×10^{13} km, for the 90% C.L. bound).

-
- [1] V. Viswanathan, A. Fienga, M. Gastineau, and J. Laskar, “INPOP17a planetary ephemerides,” *Notes Scientifiques et Techniques de l’Institut de Mecanique Celeste* **108** (2017), last Accessed: 2018-11-13.
 - [2] W. M. Folkner, J. G. Williams, D. H. Boggs, R. S. Park, and P. Kuchynka, “The Planetary and Lunar Ephemerides DE430 and DE431,” *Interplanetary Network Progress Report* **196**, 1–81 (2014).

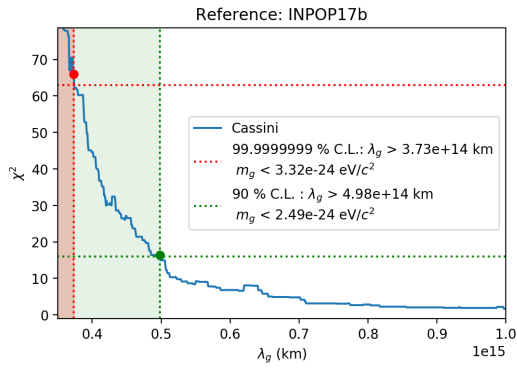


FIG. 3. Plot of $\chi^2(\lambda_g)$, and the constraints one would have deduced for λ_g without re-adjusting the Solar System parameters. It would lead to a spurious improvement of a factor 27.2 and 22.4 for the 90% and 99.9999999% C.L. bounds respectively, compared to the global fit analysis.

[3] Clifford M Will, “Solar system versus gravitational-wave bounds on the graviton mass,” *Classical and Quantum Gravity* **35**, 17LT01 (2018).